Computers and Concrete, *Vol. 16, No. 5 (2015) 669-682*
DOI: http://dx.doi.org/10.12989/cac.2015.16.5.669

Prediction of initiation time of corrosion in RC using meshless methods

Ling Yao[1a], Lingling Zhang[2], Ling Zhang[*1] and Xiaolu Li[1]

[1]*State Key Laboratory for Strength and Vibration Of Mechanical Structures, Xi'an Jiaotong University, No.28, Xianning West Road, Xi'an, Shaanxi, 710049, China*
[2]*School Of Human Settlements and Civil Engineering, Xi'an Jiaotong University, No.28, Xianning West Road, Xi'an, Shaanxi, 710049, China*

(Received July 29, 2015, Revised October 05, 2015, Accepted October 28, 2015)

Abstract. Degradation of reinforced concrete (RC) structures due to chloride penetration followed by reinforcement corrosion has been a serious problem in civil engineering for many years. The numerical simulation methods at present are mainly finite element method (FEM) and finite difference method (FDM), which are based on mesh. Mesh generation in engineering takes a long time. In the present article, the numerical solution of chloride transport in concrete is analyzed using radial point interpolation method (RPIM) and element-free Galerkin (EFG). They are all meshless methods. RPIM utilizes radial polynomial basis, whereas EFG uses the moving least-square approximation. A Galerkin weak form on global is used to attain the discrete equation, and four different numerical examples are presented. MQ function and appropriate parameters have been proposed in RPIM. Numerical simulation results are compared with those obtained from the finite element method (FEM) and analytical solutions. Two case of chloride transport in full saturated and unsaturated concrete are analyzed to test the practical applicability and performance of the RPIM and EFG. A good agreement is obtained among RPIM, EFG, and the experimental data. It indicates that RPIM and EFG are reliable meshless methods for prediction of chloride concentration in concrete structures.

Keywords: meshless method; chloride diffusion; RPIM; EFG; corrosion

1. Introduction

Reinforced concrete structures located in exposed marine environments present corrosion damage. Chloride corrosion of steel reinforcement is a main cause of deterioration of concrete structures, such as highway bridges and marine structures (Ahmad 2003, Goltermann 2003, Marchand and Samson 2009, Faramarz *et al*. 2014, Seyed *et al*. 2015). Initiation period is defined as the time for sufficient chloride penetration into the concrete cover to initiate corrosion. Therefore, developing reliable numerical methods for predicting chloride concentration is urgent to prevent deterioration of new structures and assess conditions of existing RC structures.

∗Corresponding author, Professor, E-mail: zhangl@mail.xjtu.edu.cn
[a] Ph.D. Student, E-mail: yaoling001@yahoo.com

http://www.techno-press.org/?journal=cac&subpage=8 ISSN: 1598-8198 (Print), 1598-818X (Online)

Depending on the degree of saturation, concrete can be classified as saturated or unsaturated. Chloride penetration is different in saturated and unsaturated concretes. Chloride diffusion is assumed to follow Fick's second law under the assumption that the concrete is fully saturated. Chloride penetration is complex when the concrete is unsaturated in practical engineering. Several authors proposed different models to predict chloride transport into unsaturated concrete (Guzmán *et al*. 2011, Boddy *et al*. 1999, Martın-Pérez *et al*. 2001,Conciatori *et al*. 2008). Thus, various models are analyzed with finite element method (FEM), finite difference method (FDM), and other complicated numerical methods. The common characteristic of all these methods is based on a mesh, but mesh generation that involves complex regions for actual engineering takes a long time, making mesh generation an important link of numerical modeling.

New numerical techniques called meshless methods have been developed over the past decades. Meshless methods do not require element connectivity and the integration over the solution domain requires only simple integration of cells to obtain the solution. In recent years, the method has been widely used in different areas, such as elasticity and thermal conduction fracture mechanics. Meshless method is used for the diffusion of chloride in the concrete only in (Bitaraf and Mohammadi 2008, Guo *et al*. 2012). The study in (Bitaraf and Mohammadi 2008) about a finite point method (FPM) is developed and adopted to solve the chloride diffusion equation in concrete. In (Guo *et al*. 2012), the transient meshless boundary element method is adopted to predict chloride diffusion as it places emphasis on time-dependent nonlinear coefficients. Meshless methods can be classified into three categories. The first category includes methods that need to be set up based on moving least-squares approximation. Element-free Galerkin (EFG) method (Dolbow and Belytschko 1998) and local Petrov–Galerkin method (Atluri and Zhu 1998) belong to this category. The second category includes radial point interpolation method (RPIM) with polynomial reproduction (Liu *et al*. 2005). The third class includes particle methods using the integral form approximation, such as the smoothed particle method (Randles and Libersky 1996).

RPIM and EFG are meshless methods. The governing differential equation is obtained using the Galerkin weak form, but they differ in that radial point interpolation is adopted in RPIM, whereas MLS approximation is adopted in EFG; their boundary is also enforced in different methods. The solution procedure of the RPIM is similar to that of the FEM; thus, the essential boundary conditions to be imposed are direct approach as FEM. However, Lagrange's Multiplier technique was used to impose the essential boundary conditions in the EFG method in this article.

In this article, the chloride diffusion in full saturated and unsaturated concrete is numerical simulation in RPIM and EFG methods. Section 2 briefly discusses the formulation using radial polynomial basis. Section 3 describes MLS approximation. Section 4 discusses discrete chloride diffusion model in Galerkin weak form. 1D and 2D numerical examples are then solved, discussed, and analyzed, and FEM, EFG, and RPIM results are compared in Section 5, followed by the conclusion section.

2. Radial polynomial basis in RPIM

Consider a continuous function $C(x)$ defined on a domain $\Omega \subseteq \boldsymbol{R}^d$ (d=1,2) where x is a point, Ω_s is the neighborhood of a point and $\Omega_x \subseteq \Omega$. In RPIM with polynomial reproduction, the approximation $C^h(x)$ is (Kumar and Dodagoudar 2008)

$$C(\mathbf{x}) \approx C^h(\mathbf{x}) = \sum_{i=1}^{n} \mathrm{R_i}(\mathbf{x})\mathrm{a_i} + \sum_{j=1}^{m} \mathrm{p_j}(\mathbf{x})\mathrm{b_j} = \mathbf{R}^{\mathrm{T}}(\mathbf{x})\mathbf{a} + \mathbf{P}^{\mathrm{T}}(\mathbf{x})\mathbf{b} \tag{1}$$

where $a_i(x)$ is the coefficient for $R_i(\mathbf{x})$, $R_i(\mathbf{x})$ is radial basis function, b_j is the coefficient for $p_j(\mathbf{x})$, n is the number of nodes in Ω_s of x, and m is the number of polynomial basis function, which is usually $m<n$. In 2D space, $\mathbf{P^T(x)}=[1,x,y]$. The vectors are defined as: $\mathbf{a}=[a_1,a_2,\ldots a_n]^{\mathbf{T}}$; $\mathbf{b}=[b_1,b_2,\ldots b_m]^{\mathbf{T}}$; $\mathbf{R^T(x)}=[R_1(\mathbf{x}),R_2(\mathbf{x}),\ldots R_n(\mathbf{x})]$; $\mathbf{P^T(x)}=[p_1(\mathbf{x}),p_2(\mathbf{x}),\ldots p_m(\mathbf{x})]$. The coefficients a_i and b_j in Eq. (1) are determined by enforcing the interpolation pass through all $\boldsymbol{n}$-scattered nodal points within the influence domain. The matrix form of Eq. (1) is expressed as: To guarantee the uniqueness of the approximate function, the coefficient of additional conditions is as Eq.(2)

$$\mathbf{C^e=R_0a+Pb} \tag{2}$$

$$\sum_{i=1}^{n} \boldsymbol{p_j}(\mathrm{x})\boldsymbol{a_i} = 0 \quad \boldsymbol{j} = 1,2,\ldots,\boldsymbol{m} \tag{3}$$

The matrix form of Eq. (3) is

$$\mathbf{P^Ta=0} \tag{4}$$

Combining Eq. (2) and Eq. (4), Eq. (2) is expressed in matrix form as follows

$$\begin{bmatrix} \mathbf{R_0} & \mathbf{P} \\ \mathbf{P^T} & \mathbf{0} \end{bmatrix} \begin{Bmatrix} \mathbf{a} \\ \mathbf{b} \end{Bmatrix} = \begin{Bmatrix} \mathbf{C^e} \\ \mathbf{0} \end{Bmatrix} \tag{5}$$

where

$$\mathbf{C^e} = [\boldsymbol{C_1},\boldsymbol{C_2},\ldots,\boldsymbol{C_n}]^{\mathrm{T}} \tag{6}$$

$$\mathbf{P^T} = \begin{bmatrix} 1 & 1 & \ldots & 1 \\ \boldsymbol{x}_1 & \boldsymbol{x}_2 & \ldots & \boldsymbol{x}_n \\ \boldsymbol{y}_1 & \boldsymbol{y}_2 & \ldots & \boldsymbol{y}_n \end{bmatrix} \tag{7}$$

$$\mathbf{R_0} = \begin{bmatrix} \boldsymbol{R}_1(\boldsymbol{r}_1) & \boldsymbol{R}_2(\boldsymbol{r}_1) & \ldots & \boldsymbol{R}_n(\boldsymbol{r}_1) \\ \boldsymbol{R}_1(\boldsymbol{r}_2) & \boldsymbol{R}_2(\boldsymbol{r}_2) & \ldots & \boldsymbol{R}_n(\boldsymbol{r}_2) \\ \vdots & \vdots & \vdots & \vdots \\ \boldsymbol{R}_1(\boldsymbol{r}_n) & \boldsymbol{R}_2(\boldsymbol{r}_n) & \cdots & \boldsymbol{R}_n(\boldsymbol{r}_n) \end{bmatrix}_{\boldsymbol{n}\times\boldsymbol{n}} \tag{8}$$

It can be attained from Eq. (1)

$$\mathbf{a} = \mathbf{R_0^{-1}C^e} - \mathbf{R_0^{-1}Pb} \tag{9}$$

$$\mathbf{b} = \mathbf{S_b C^e} = \left[\mathbf{P^T R_0^{-1} P}\right]^{-1} \mathbf{P^T R_0^{-1} C^e} \tag{10}$$

Combing Eq. (9) and Eq.(10)

$$\mathbf{a}=\mathbf{S}_a\mathbf{C}^e \tag{11}$$

where

$$\mathbf{S}_a = \mathbf{R}_0^{-1}[1 - \mathbf{P}\mathbf{S}_b] = \mathbf{R}_0^{-1} - \mathbf{R}_0^{-1}\mathbf{P}\mathbf{S}_b \tag{12}$$

Substituting Eq. (10) and Eq. (11) in Eq. (1) yields

$$C(\mathbf{x}) = [\mathbf{R}^{\mathrm{T}}\mathbf{S}_a + \mathbf{P}^{\mathrm{T}}\mathbf{S}_b]\mathbf{C}^e = \mathbf{\Phi}(\mathbf{x})\mathbf{C}^e \tag{13}$$

where

$$\mathbf{\Phi}(\mathbf{x}) = [\Phi_1(\mathbf{x}), \Phi_2(\mathbf{x}), \ldots \Phi_n(\mathbf{x})] \tag{14}$$

The derivatives of shape function are

$$\begin{cases} \dfrac{\partial \Phi_k}{\partial x} = \displaystyle\sum_{i=1}^{n} \frac{\partial R_i}{\partial x}\mathbf{S}_{ik}^a + \sum_{j=1}^{m} \frac{\partial P_j}{\partial x}\mathbf{S}_{jk}^b \\ \dfrac{\partial \Phi_k}{\partial y} = \displaystyle\sum_{i=1}^{n} \frac{\partial R_i}{\partial y}\mathbf{S}_{ik}^a + \sum_{j=1}^{m} \frac{\partial P_j}{\partial y}\mathbf{S}_{jk}^b \end{cases} \tag{15}$$

In this article, the thin plate spline (TPS) radial basis and multi-quadrics (MQ) are adopted (Li *et al*. 2003). The radial basis function is only related with the distance r_i as follows

$$r_i = \sqrt{(x - x_i)^2 + (y - y_i)^2} \tag{16}$$

MQ function

$$\mathbf{R}_i(\mathbf{x}) = \mathbf{R}_i(r_i) = (r_i^2 + (\alpha_c d_c)^2)^q = [(x - x_i)^2 + (y - y_i)^2 + (\alpha_c d_c)^2]^q \tag{17}$$

TPS function

$$\mathbf{R}_i(\mathbf{x}) = \mathbf{R}_i(r_i) = (r_i^2)^\eta = [(x - x_i)^2 + (y - y_i)^2]^\eta \tag{18}$$

where α_c, q, and η are shape parameters and d_c is the average distance between two nodes in Ω_s. Their partial derivatives are obtained as follows

$$\begin{cases} \dfrac{\partial R_i}{\partial x} = 2q(r_i^2 + (\alpha_c d_c)^2)^{q-1}(x - x_i) \\ \dfrac{\partial R_i}{\partial y} = 2q(r_i^2 + (\alpha_c d_c)^2)^{q-1}(y - y_i) \end{cases}$$

$$\begin{cases} \dfrac{\partial R_i}{\partial x} = 2\eta(r_i^2)^{\eta-1}(x - x_i) \\ \dfrac{\partial R_i}{\partial y} = 2\eta(r_i^2)^{\eta-1}(y - y_i) \end{cases} \tag{19}$$

3. MLS approximation in EFG

In the MLS approximation, $u(x)$ is assumed to be set as a field function in the support domain Ω. The approximation of $C(x)$ at point x is denoted by $C^h(x)$ (Boddy *et al*. 1999) as

$$C^h(\mathbf{x}) = \sum_{i=1}^{m} p_i(\mathbf{x}) a_i(\mathbf{x}) = \mathbf{p}^{\mathbf{T}}(\mathbf{x})\mathbf{a}(\mathbf{x}) \tag{20}$$

where

$$\mathbf{a}(\mathbf{x}) = [a_1(\mathbf{x}), a_2(\mathbf{x}), \ldots a_n(\mathbf{x})]^{\mathbf{T}} \tag{21}$$

$$\mathbf{p}^{\mathbf{T}}(\mathbf{x}) = \mathbf{p}^{\mathbf{T}}(x, y) = [1, x, y, xy, x^2, y^2, \cdots, x^k, y^k] \tag{22}$$

The undetermined coefficients $\mathbf{a}(\boldsymbol{x})$ are obtained by minimizing the function $\boldsymbol{J}$

$$\boldsymbol{J} = \sum_{\boldsymbol{I}=1}^{\boldsymbol{N}} \boldsymbol{w}_{\boldsymbol{I}}(\boldsymbol{x} - \boldsymbol{x}_{\boldsymbol{I}})[\boldsymbol{C}^{\boldsymbol{h}}(\boldsymbol{x}, \boldsymbol{x}_{\boldsymbol{I}}) - \boldsymbol{C}(\boldsymbol{x}_{\boldsymbol{I}})]^2 = \sum_{\boldsymbol{I}=1}^{\boldsymbol{N}} \boldsymbol{w}_{\boldsymbol{I}}(\boldsymbol{x} - \boldsymbol{x}_{\boldsymbol{I}})[\sum_{\boldsymbol{i}=1}^{\boldsymbol{m}} \mathbf{p}^{\mathbf{T}}(\boldsymbol{x}_{\boldsymbol{I}})\mathbf{a}(\boldsymbol{x}) - \boldsymbol{C}(\boldsymbol{x}_{\boldsymbol{I}})]^2 \tag{23}$$

The sationarity of $\boldsymbol{J}$ in Eq. (23) with respect to $\mathbf{a}(\boldsymbol{x})$ results in the following equations

$$\boldsymbol{A}(\boldsymbol{x})\boldsymbol{a}(\boldsymbol{x}) = \boldsymbol{B}(\boldsymbol{x})\boldsymbol{C} \tag{24}$$

$$\mathbf{a}(\mathbf{x}) = \mathbf{A}^{-1}(\mathbf{x})\mathbf{B}(\mathbf{x})\mathbf{C} \tag{25}$$

$$\boldsymbol{A}(\mathbf{x}) = \sum_{\boldsymbol{I}=1}^{\boldsymbol{N}} \boldsymbol{W}_{\boldsymbol{I}}(\boldsymbol{x})\boldsymbol{p}(\boldsymbol{x}_{\boldsymbol{I}})\boldsymbol{p}^{\boldsymbol{T}}(\boldsymbol{x}_{\boldsymbol{I}}) \tag{26}$$

$$\boldsymbol{B}(\mathbf{x}) = [\boldsymbol{w}_1(\boldsymbol{x})\boldsymbol{p}(\boldsymbol{x}_1)\boldsymbol{w}_2(\boldsymbol{x})\boldsymbol{p}(\boldsymbol{x}_2)\ldots\boldsymbol{w}_{\boldsymbol{N}}(\boldsymbol{x})\boldsymbol{p}(\boldsymbol{x}_{\boldsymbol{N}})] \tag{27}$$

$$C^h(\mathbf{x}) = \mathbf{p}^{\mathbf{T}}(\mathbf{x})\mathbf{a}(\mathbf{x}) = \mathbf{p}^{\mathbf{T}}(\mathbf{x})\mathbf{A}^{-1}(\mathbf{x})\mathbf{B}(\mathbf{x})\mathbf{C} \tag{28}$$

4. Discretization of governing equation

Chloride diffusion in full saturated concrete is generally assumed to follow Fick's second law (Bitaraf and Mohammadi 2008). The diffusion equation is written as

$$\frac{\partial C}{\partial t} = D_x \frac{\partial^2 C}{\partial x^2} + D_y \frac{\partial^2 C}{\partial y^2} \tag{29}$$

where $C=C(x, y, t)$ represents concentration, t is time, and D_x and D_y are diffusion coefficient in x- and y-directions, respectively.

The initial and boundary conditions are

$$C(x, y, 0) = C_0 \qquad \text{in } \Omega \tag{30}$$

$$C = C_s \qquad \text{on } \Gamma_1 \tag{31}$$

The weighted integral form of Eq. (29) with Galerkin weak form on global is expressed as

$$\int_\Omega \delta C^{\mathrm{T}} D_x \frac{\partial^2 C}{\partial x^2} d\Omega + \int_\Omega \delta C^{\mathrm{T}} D_y \frac{\partial^2 C}{\partial y^2} d\Omega - \int_\Omega \delta C^{\mathrm{T}} \frac{\partial C}{\partial t} d\Omega = 0 \tag{32}$$

By using divergence theorem and natural boundary conditions

$$\int_\Omega \delta \frac{\partial C^{\mathrm{T}}}{\partial x} D_x \frac{\partial C}{\partial x} d\Omega + \int_\Omega \delta \frac{\partial C^{\mathrm{T}}}{\partial y} D_y \frac{\partial C}{\partial y} d\Omega + \int_\Omega \delta C^{\mathrm{T}} \frac{\partial C}{\partial t} = 0 \tag{33}$$

Substituting Eq. (13) or Eq. (28) into Eq. (32) yields

$$\int_\Omega \mathbf{\Phi}_{,x}^{\mathrm{T}} \delta C^{\mathrm{T}} D_x \mathbf{\Phi}_{,x} C \; d\Omega + \int_\Omega \mathbf{\Phi}_{,y}^{\mathrm{T}} \delta C^{\mathrm{T}} D_y \mathbf{\Phi}_{,y} C \; d\Omega + \int_\Omega \mathbf{\Phi}^{\mathrm{T}} \delta C^{\mathrm{T}} \mathbf{\Phi} C_{,t} \; d\Omega = 0 \tag{34}$$

The matrix form of Eq. (34) are written as

$$[M]\{C\}_{,t} + [K]\{C\} = 0 \tag{35}$$

$$\mathbf{M}_{IJ} = \int_\Omega \begin{bmatrix} \Phi_I \\ \Phi_J \end{bmatrix}^{\mathrm{T}} \begin{bmatrix} \Phi_I \\ \Phi_J \end{bmatrix} d\Omega \tag{36}$$

$$\mathbf{K}_{IJ} = \int_\Omega \begin{bmatrix} \Phi_{I,x} \\ \Phi_{J,y} \end{bmatrix}^{\mathrm{T}} \begin{bmatrix} D_x & 0 \\ 0 & D_y \end{bmatrix} \begin{bmatrix} \Phi_{I,x} \\ \Phi_{J,y} \end{bmatrix} d\Omega \tag{37}$$

Galerkin approach is applied to solve the weak form; thus, integrating over the problem domain is necessary. Gauss quadrature scheme is used for integration.

Using Crank-Nicolson technique for time approximation, Eq. (35) can be written as

$$\mathbf{K}_{eff} \mathbf{C}^n = \mathbf{f}^n \tag{38}$$

where

$$\mathbf{K}_{eff} = \mathbf{M} + \frac{\Lambda t}{2} \mathbf{K} \tag{39}$$

$$\mathbf{f}^n = \{\mathbf{C}\}^{n-1} \left([\mathbf{M}] - \frac{\Delta t}{2} [\mathbf{K}]\right) \tag{40}$$

Chloride diffusion follows Fick's second law when the concrete is fully saturated in concrete, whereas diffusion is not only a transport mechanism but also other absorption mechanism in

non-saturated concrete. The author proposed convection-diffusion models to predict chloride transport in unsaturated concrete. The convection-diffusion equation for divergence-free velocity field is given by (Da Costa *et al*. 2013)

$$\frac{\partial C}{\partial t} = D\frac{\partial^2 C}{\partial x^2} - \mu\frac{\partial C}{\partial x} \tag{41}$$

K is different from Eq. (37) and other parameter is the same in unsaturated concrete.

$$\mathbf{K}_{IJ} = \int_{\Omega}\begin{bmatrix}\Phi_{I,x}\\ \Phi_{J,y}\end{bmatrix}^{\mathrm{T}}\begin{bmatrix}D_x & 0\\ 0 & D_y\end{bmatrix}\begin{bmatrix}\Phi_{I,x}\\ \Phi_{J,y}\end{bmatrix}d\Omega + \begin{bmatrix}\Phi_I\\ \Phi_J\end{bmatrix}\mu\begin{bmatrix}\Phi_{I,x}\\ \Phi_{J,x}\end{bmatrix}d\Omega \tag{42}$$

5. Numerical examples

Applications of RPIM and EFG are illustrated using four examples that deal with chloride diffusion in concrete. MATLAB codes are developed to obtain EFG and RPIM results, and FEM results are obtained using COMSOL Multiphysics 4.3 software.

5.1 1D Chloride diffusion in full saturated concrete

The first example is a 0.15 m×0.15 m concrete slab. The left boundary of the slab is subjected to a chloride concentration of 5% (by mass of NaCl). The top and bottom walls are isolated. The initial chloride concentration is 0. In this problem, the diffusion coefficient is assumed in the first example to be a constant D=1.5768×10^{-12} m^2/s, and in the second example to be a time-dependent function $D(t) = D_0(\frac{t_0}{t})^m$ (Luping and Gulikers 2007). D_0 is the diffusion coefficient at some reference time t_0, and m_0 denotes the material constant. In this problem, D=1.5768×10^{-12}×(0.1/t)$^{0.1}$ m^2/s. For the purpose of convergence studies, the root-mean square (RMS) error is defined as: $R = \frac{1}{n}\sqrt{\sum_{I=1}^{n} C(x_I) - C^*(x_I)}$, where n is the number of sample points. $C(x_1)$ is the calculation with meshless methods, and $C^*(x_1)$ denotes the analytical solution.

5.1.1 Coefficient D is a constant in 1D

The analytical solution for 1D diffusion behavior of chloride ions in concrete is

$$C(x,t) = C_s(1 - erf(\frac{x}{2\sqrt{Dt}})) \tag{43}$$

where *erf* (.) is the error function and C_s=5%. To implement the meshless method, the slab is discretized into 31 nodes at exposure time t=20 years. Table 1 gives a numerical comparison of the RMS errors for different radial basis functions. Notably, minimum error occurs when using MQ function and q=0.98; thus, we choose MQ function and q=0.98 in the numerical simulation that follows.

Table 1 RMS(%) error of different radial basis functions at nodes=31 exposed time t=20 years

MQ(α_c=2.0)		TPS	
q	Error (%)	η	Error (%)
-0.50	0.0786	1.05	0.2102
0.50	0.0762	1.25	0.1689
0.98	0.0727	1.50	0.1290
1.01	0.0728	1.75	0.1002
1.20	0.0732	1.95	0.0847

Table 2 Results of RPIM, EFG, FEM and exact at a few specific locations (31nodes, t=20years)

Location (m)	Chloride concentration (%)			
x	RPIM	EFG	FEM	Exact
0.01	4.1120	4.1132	4.1174	4.1129
0.03	2.5106	2.5067	2.5110	2.5058
0.05	1.3168	1.3134	1.3096	1.3112
0.07	0.5865	0.5855	0.5800	0.5826
0.09	0.2201	0.2207	0.2182	0.2180
0.11	0.0693	0.0702	0.0690	0.0682
0.13	0.0189	0.0196	0.0186	0.0178
0.15	0.0081	0.00087	0.007637	0.0039

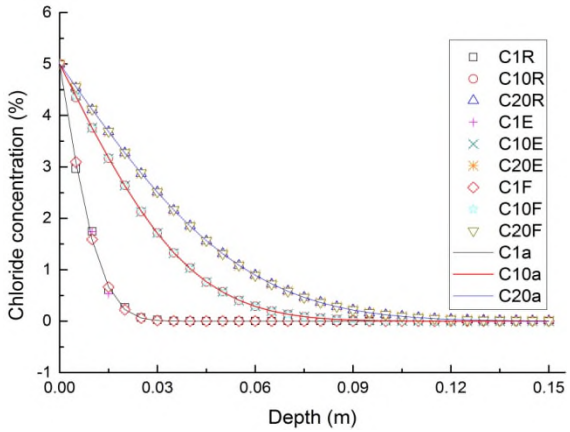

Fig. 1 Variation of chloride concentration with depth

Table 2 shows a comparison of the chloride concentration by using the RPIM, EFG, and FEM methods and the exaction solution at a few specific locations among the 31 nodes at t=20 years. The same number of nodes was used in all methods. Table 2 shows that the results of the meshless methods are very closer to the analytical solutions than FEM, although all errors are very small.

Chloride concentration change with depth at exposure times of 1, 10, and 20 years is shown in Fig. 1. In this figure, C1R, C1E, C1F and C1a denote the chloride concentration from RPIM, EFG, FEM and the analytical solution after one year's exposure employing 31 nodes. Results of the

Table 3 Chloride concentration RMS error at time t=20 years (D is a constant)

	Number of nodes	RPIM	EFG
RMS (%)	16	0.1773	0.1766
	31	0.0727	0.0622

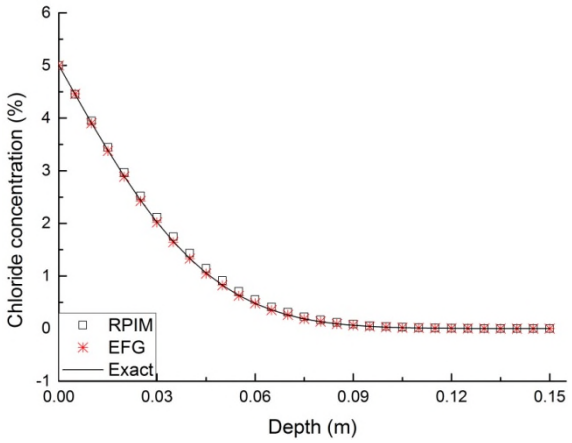

Fig. 2 Chloride concentration-depth at time=20 years (at nodes=31)

Table 4 The initiation period of corrosion by different methods

	Number of nodes		RPIM	EFG	FEM	Exact
D is a constant	16	initiation period (year)	9.10	9.20	9.30	9.20
	31		9.25	9.25	9.35	9.20
D is a time-dependent function	16	initiation period (year)	12.05	13.55	13.75	-
	31		12.50	13.65	13.85	-

RPIM, EFG and FEM are nearly identical with the analytical results. By decreasing the number of nodes to 16, the error of numerical methods at time t=20 years is illustrated in Table 3.

5.1.2 Coefficient D is a time-dependent function in 1D

In the second example, when the coefficient D is a time-dependent function, the analytical solution is represented by (Suryavanshi *et al*. 2002)

$$\frac{C}{C_s}=(1-erf(\frac{x}{2\sqrt{D_a\cdot t}}) \tag{44}$$

where $D_a=\frac{D_0}{1-m}[(1+\frac{t_0}{t})^{1-m}-(\frac{t_0}{t})^{1-m}](\frac{t_0}{t})^m$.

The transient chloride diffusion in concrete is shown in Fig. 2. Results shown in Fig. 2 indicate good agreement among the RPIM and EFG methods and the analytical solution. The RMS error was 0.9215% between the RPIM and the analytical result, and the RMS error of the EFG method was 0.0865% when t=20 years and 31 nodes were used. The accuracy of the EFG is higher than

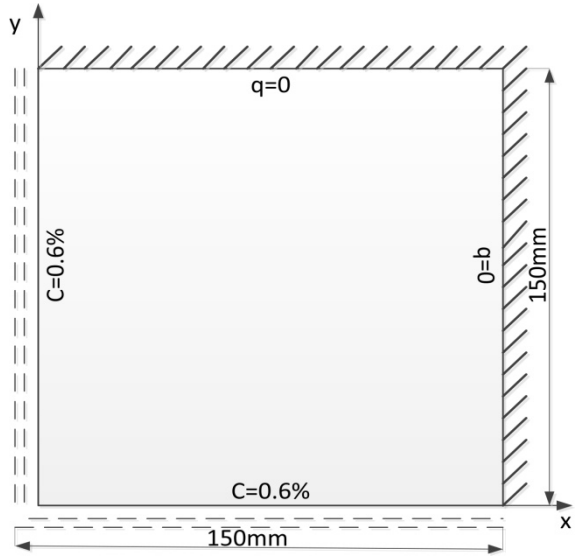

Fig. 3 2D square concrete

that of RPIM, but the error of RPIM is still poor in an actual engineering application. Selecting the critical chloride ion content (C_t) of 0.5% and a depth of 5 cm, the initiation period of corrosion for the start of rebar is shown in Table 4. It is clear that prediction of the initiation periods of corrosion in different methods are very close to the exact.

From these results of two examples, RPIM and EFG are effective in predicting chloride diffusion in concrete whether D is a constant or not.

5.2 2D problems in full saturated concrete

The rate of chloride diffusion in an actual reinforced concrete structure is very slow, so measuring diffusion is a slow and time-consuming process. In addition, studies that deal with chloride diffusion over long periods are few. In this section, a concrete plate of 0.15 m×0.15 m was used as an example in actual engineering (Fig. 3). The left and bottom boundaries of the plate were subjected to a chloride concentration of 0.6% as Dirichlet's boundaries, and the right and top boundaries were isolated. The initial chloride concentration was 0 similar to that reported in (Guo *et al*. 2012).

5.2.1 Coefficient D is a constant in 2D

A regular distribution of 31×31 nodes was selected in the Ω domain for all methods. Given the 2D characteristic of the example, when the diffusion coefficient D is a constant (D=9.38×10^{-12} m^2/s), the analytical solution is as follows (Luping and Gulikers 2007)

$$C(x,y,t) = C_s[1 - erf(\frac{x}{2\sqrt{D_x t}})erf(\frac{y}{2\sqrt{D_y t}})] \tag{45}$$

Here, the selected exposed time t is 3, 5, and 10 years. Variations of chloride concentration from the lower-left corner to the upper-right corner and the analytical solution at the same position

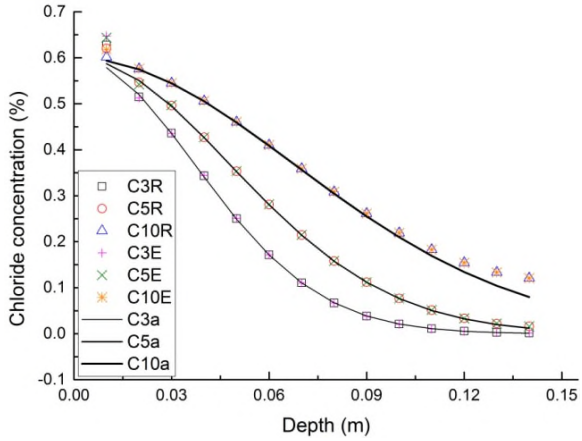

Fig.4 Variations of chloride concentration at diagonal points

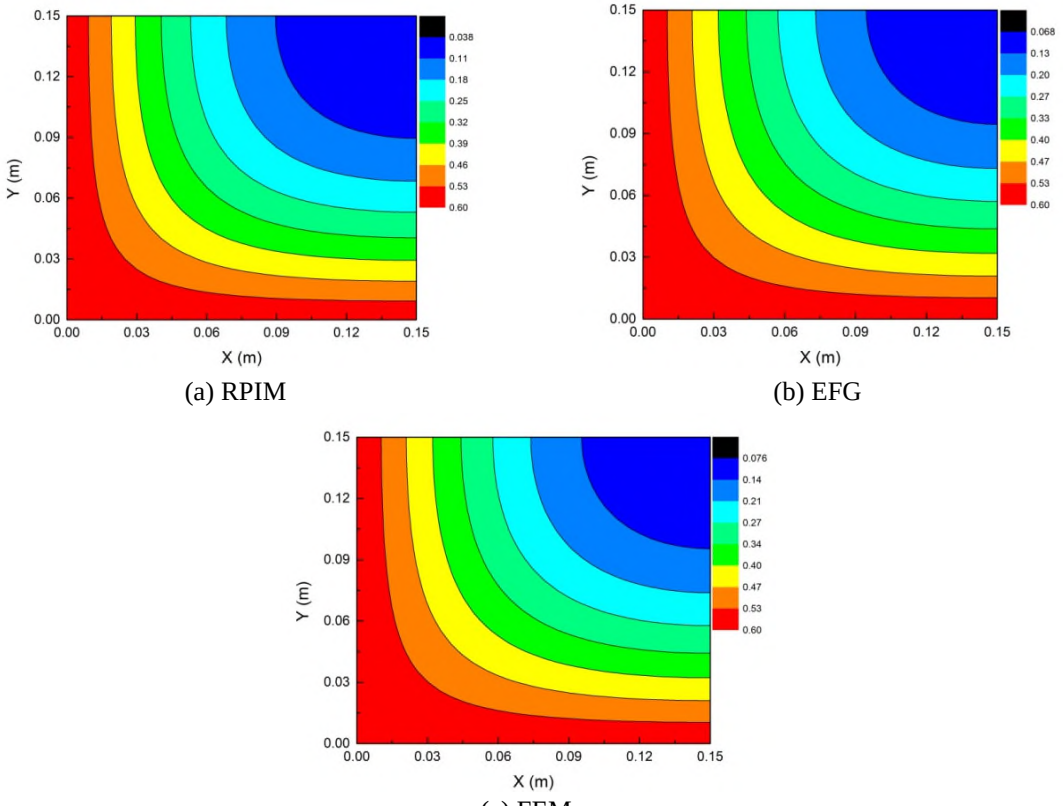

(a) RPIM (b) EFG

(c) FEM

Fig. 5 Distribution of chloride concentration in (a), (b) and (c) methods after exposed time t=20 years

on the plate are shown in Fig. 4. The relative error of the chloride concentration at diffusion depth of 50 mm, for instance, is about 0.48%, 0.20%, and 0.19% after 3, 5, and 10 year's exposure in RPIM, respectively.

Table 5 The initiation period of corrosion by different methods

Initiation period (year)	RPIM	EFG	FEM	Exact
D is a constant	7.50	7.45	7.45	7.46
D is a time-dependent function	23.00	22.00	18.20	-

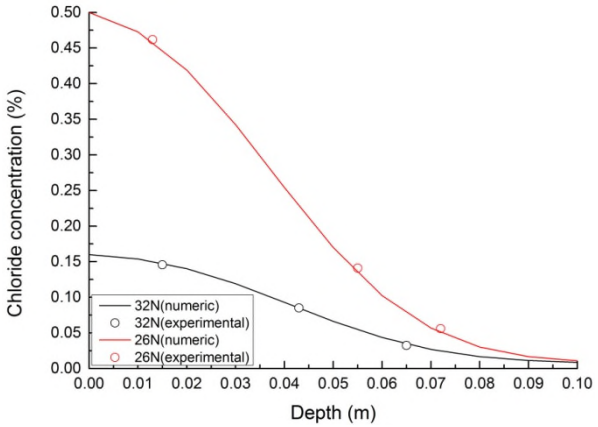

Fig. 6 Variations of chloride concentration at diagonal points

5.2.2 Coefficient D is a time-dependent function in 2D

To verify the efficiency of the RPIM, concrete coefficient D is chosen as a time-dependent function $D=9.62\times10^{-12}\times(0.1/t)^{0.2}$ m^2/s. Other conditions are the same as the previous 2D problem. Fig. 5 shows the distribution of chloride concentration at an exposure time of t=20years with the RPIM, EFG, and FEM methods. Results from RPIM and EFG are roughly the same with FEM and the direction of chloride diffusion is consistent. Chloride concentration increases significantly near the two exposed surface and diagonal points.

If we choose C_t=0.3% and assume that a rebar exists at a depth of 7 cm, then a critical concentration on the rebar surface is reached in about 3 years. The initiation period for the start of rebar corrosion is shown in Table 5. These results show good agreement among the meshless RPIM, EFG, and FEM methods.

5.3 Chloride diffusion in unsaturated concrete

In most real situations, chloride transport is not attributed exclusively to a diffusion mechanism (Conciatori *et al*. 2008). Some authors propose convection-diffusion models to predict chloride transport in unsaturated concrete. The experimental data are from 25 years of service life in marine environments. Fig. 6 shows that the RPIM method solution fitted to the experiment given in (Da Costa *et al*. 2013). Results obtained from the RPIM for the prediction of chloride transport in unsaturated concrete is stable and accurate.

5.4 Chloride diffusion in real concrete

Experimental results of 18 RC blocks exposed in the splash zone on the southeast coast of England (Thomas and Bamforth 1999) are compared with numerical results from RPIM and EFG

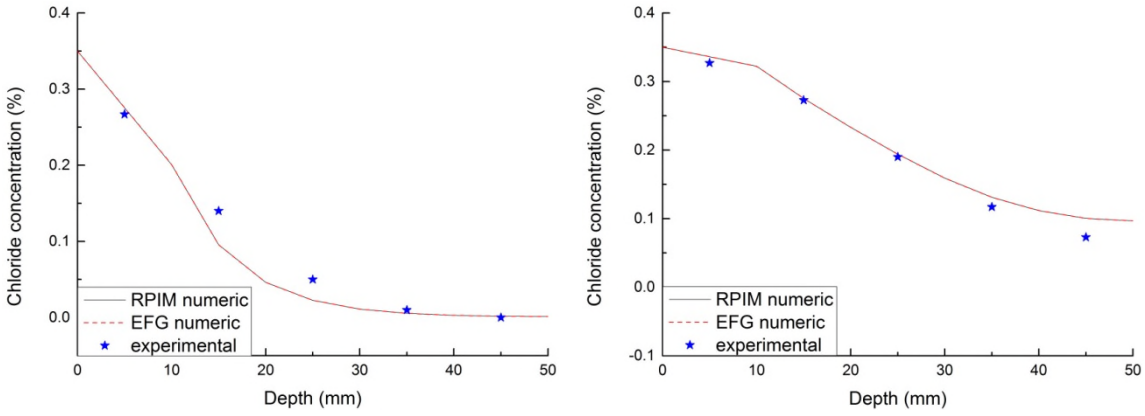

(a) 0.5 year (b) 3 year

Fig. 7 Distribution of chloride concentration with penetration depth after (a) 0.5 (b) 3 year's exposure

methods. Fig. 7 for PC shows the variation of chloride concentration at t=0.5 and 3 years. Result indicates that the RPIM and EFG of numerical method better agree with the experimental results as time increases.

6. Conclusions

RPIM and EFG are meshless methods based on the discretization of the governing equation in Galerkin weak form. These methods can effectively solve chloride diffusion in concrete. The implementation of these methods is simple and similar to each other. Results obtained using RPIM and EFG were compared with FEM and the analysis shows that RPIM results obtained using the proposed MQ function and EFG results are in good agreement with those obtained using FEM. The practical applicability of the RPIM is demonstrated with two experimental cases. 1D and 2D simulations demonstrated that the accuracy of RPIM is lower than EFG, but the error is still small in practical engineering. RPIM is still applicable to chloride transport in the unsaturated concrete. From these examples, it looks good to indicate that meshless numerical approaches compared with an analytical solution whose parameters are fitted to measured chloride profile. It also shows a good agreement among the RPIM, EFG methods and the analytical solution when the boundary conditions are constant in all examples. This work can be also extended for chloride diffusion of 3D structures.

References

Ahmad, S. (2003), "Reinforcement corrosion in concrete structures, its monitoring and service life prediction-a review ", *Cem. Concr. Compos.*, **25**(4), 459-471.

Atluri, S. and Zhu, T. (1998), "A new meshless local Petrov-Galerkin (MLPG) approach in computational mechanics", *Comput. Mech.*, **22**(2), 117-127.

Bitaraf, M. and Mohammadi, S. (2008), "Analysis of chloride diffusion in concrete structures for prediction of initiation time of corrosion using a new meshless approach", *Constr. Build. Mater.*, **22**(4), 546-556.

Boddy, A., Bentz, E., Thomas, M. and Hooton, R. (1999), "An overview and sensitivity study of a

multimechanistic chloride transport model", *Cement Concrete Res.*, **29**(6), 827-837.
Conciatori, D., Sadouki, H. and Brühwiler, E. (2008), "Capillary suction and diffusion model for chloride ingress into concrete", *Cement Concrete Res.*, **38**(12), 1401-1408.
Da Costa, A., Fenaux, M., Fernández, J., Sánchez, E. and Moragues, A. (2013), "Modelling of chloride penetration into non-saturated concrete: case study application for real marine offshore structures", *Constr. Build. Mater.*, **43**, 217-224.
Dolbow, J. and Belytschko, T. (1998), "An introduction to programming the meshless Element F reeGalerkin method", *Arch. Comput. Method E.*, **5**(3), 207-241.
Faramarz, M., Aliakbar, R. and Ehsan, J. (2014), "Assessment of some parameters of corrosion initiation prediction of reinforced concrete in marine environments", *Comput. Concrete*, **13**(1),71-82.
Goltermann, P. (2003), "Chloride ingress in concrete structures: Extrapolation of observations", *ACI Mater. J.*, **100**(2),114-119.
Guo, L., Chen, T. and Gao, X.W. (2012) , "Transient meshless boundary element method for prediction of chloride diffusion in concrete with time dependent nonlinear coefficients", *Eng. Anal. Bound. Elem.*, **36**(2), 104-111.
Guzmán, S., Gálvez, J.C. and Sancho, J.M. (2011), "Cover cracking of reinforced concrete due to rebar corrosion induced by chloride penetration", *Cement Concrete Res.*, **41**(8), 893-902.
Kumar, R.P. and Dodagoudar, G. (2008), "Two-dimensional modelling of contaminant transport through saturated porous media using the radial point interpolation method (RPIM)", *Hydrogeol. J.*, **16**(8), 1497-1505.
Li, J., Chen, Y. and Pepper, D. (2003), "Radial basis function method for 1-D and 2-D groundwater contaminant transport modeling", *Comput. Mech.*, **32**(1), 10-15.
Liu, G.R., Zhang, G., Gu, Y. and Wang, Y. (2005), "A meshfree radial point interpolation method (RPIM) for three-dimensional solids", *Comput. Mech.*, **36**(6), 421-430.
Luping, T. and Gulikers, J. (2007),"On the mathematics of time-dependent apparent chloride diffusion coefficient in concrete", *Cement Concrete Res.*, **37**(4), 589-595.
Marchand, J. and Samson, E. (2009), "Predicting the service-life of concrete structures–limitations of simplified models", *Comput. Mech.*, **31**(8), 515-521.
Martın-Pérez, B., Pantazopoulou, S. and Thomas, M. (2001), "Numerical solution of mass transport equations in concrete structures ", *Comput. Struct.*, **79**(13), 1251-1264.
Randles, P. and Libersky, L. (1996), "Smoothed particle hydrodynamics: Some recent improvements and applications", *Comput. Method. Appl. M.*, **139**(1), 375-408.
Suryavanshi, A.K., Swamy, R.N. and Cardew, G.E. (2002), "Estimation of diffusion coefficients for chloride ion penetration into structural concrete", *ACI Mater. J.*, **99**(5), 441-449.
Seyed, A.H., Naser, S. and Seyed,S.M. (2015), "Correlation between chloride-induced corrosion initiation and time to covercracking in RC Structures", *Struct. Eng. Mech.*, **56**(2), 257-273.
Thomas, M.D. and Bamforth, P.B. (1999), "Modelling chloride diffusion in concrete: effect of fly ash and slag", *Cement Concrete Res.*, **29**(4), 487-495.

CC